Orbital ordering and valence states in $(La_{1+x}Ca_{1-x})CoRuO_6$ double perovskites

Jan-Willem G. Bos
Department of Chemistry, University of Cambridge, Lensfield Road, Cambridge, CB2 1EW, United Kingdom

J. Paul Attfield
Centre for Science at Extreme Conditions and School of Chemistry, University of Edinburgh, West Mains Road, Edinburgh, EH9 3JJ, United Kingdom

Ting-Shan Chan and Ru-Shi Liu
Department of Chemistry and Center for Nano Storage Research, National Taiwan University, Taipei 106, Republic of China

Ling-Yun Jang
National Synchrotron Radiation Research Center, Hsinchu 300, Taiwan, Republic of China
(Received 7 December 2004; revised manuscript received 8 March 2005; published 1 July 2005)

$(La_{1+x}Ca_{1-x})CoRuO_6$ double perovskites have been studied by neutron diffraction and x-ray absorption spectroscopy. The thermal evolution of the $(LaCa)CoRuO_6$ structure has been investigated between 4 and 1073 K using neutron powder diffraction. The cell b axis shows a crossover from negative to positive thermal expansion at $T \approx 425$ K, which is accompanied by a discontinuity in the c axis. This is shown to result from a partial orbital ordering of the Co^{2+} t_{2g} holes. Ru valence states of doped $(La_{1+x}Ca_{1-x})CoRuO_6$ $(-0.25 \leqslant x \leqslant 0.25)$ materials have been investigated using XANES spectroscopy. Electron-doping $(x > 0)$ leads to reduction of $Ru^{5+} \rightarrow Ru^{4+}$ while hole-doped $x \leqslant 0$ compositions have a constant Ru^{5+} state. These observations support a proposed asymmetric doping model.

DOI: 10.1103/PhysRevB.72.014101 PACS number(s): 61.50.Ks, 61.12.Ld, 61.10.Ht, 61.66.Fn

I. INTRODUCTION

Many double perovskites with B-site ordering of transition metals are known,[1] some of which, e.g., Sr_2FeMoO_6 and Sr_2FeReO_6 (Refs 2 and 3), are found to be itinerant ferrimagnets that display large low field magnetoresistances. The itinerancy and ferrimagnetism arise from a spin-polarized conduction mechanism in which ordering and electronic configurations of the transition metal cations play a critical role.[4] Structurally, the 3d and the 4d or 5d transition metal cations are ordered in an alternating (rock salt) manner within a perovskite lattice. Electronically, the 3d cation has a large spin ($S=2$ to 5/2 for Fe^{2+}-Fe^{3+}) whereas the 4d or 5d cation usually has $S \leqslant 1$. Equal spins of the 3d and 4 or 5d cations could result in a so-called half-metallic antiferromagnet (HMAF), where completely spin-polarized conduction occurs in a zero magnetization material.[5] Candidate HMAF double perovskite materials are, for example, $(LaA)CoRuO_6$ where both (high-spin) Co^{2+} and Ru^{5+} have $S=3/2$. However, previous studies showed that these materials order antiferromagnetically with two opposed Co and two opposed Ru spin sublattices. They are variable range hopping semiconductors, with $T_N=96$ K for $A=$Ca and 85 K for $A=$Sr, and show no magnetotransport effects.[6,7] Excess A-cation substitution (hole doping) results in a rapid reduction of the resistivity while the Neel temperature increases only moderately. Electron doping leads to a strong reduction of T_N but has little effect on the resistivity. Structurally, the Co/Ru antisite disorder increases rapidly for hole doping and Sr_2CoRuO_6 is completely cation disordered.[8] Excess La substitution reduces the cation ordering much less significantly and La_2CoRuO_6 is found to have an ordered arrangement of Co and Ru.[9]

Here, we present the results of a variable temperature $(4 \leqslant T \leqslant 1073$ K) neutron powder diffraction study on $(LaCa)CoRuO_6$. In addition, the Ru valences of the $(La_{1+x}Ca_{1-x})CoRuO_6$ $(-0.25 \leqslant x \leqslant 0.25)$ solid solution have been investigated using x-ray absorption near edge structure (XANES) spectroscopy.

II. EXPERIMENTAL

The synthesis of the $(La_{1+x}Ca_{1-x})CoRuO_6$ $(-0.25 \leqslant x \leqslant 0.25)$ samples has been described in a previous

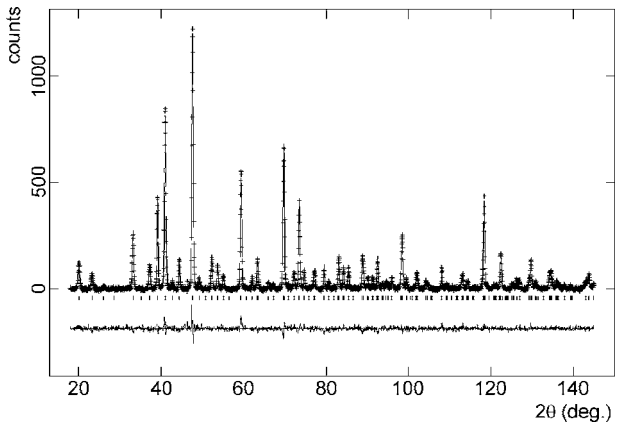

FIG. 1. The observed (crosses), calculated (full line) and difference (bottom) NPD Rietveld profiles for $(LaCa)CoRuO_6$ at 1073 K. (Residuals: $\chi^2=2.31$, $wRp=4.76\%$, $Rp=3.75\%$, and $R_F^2=5.35\%$.)

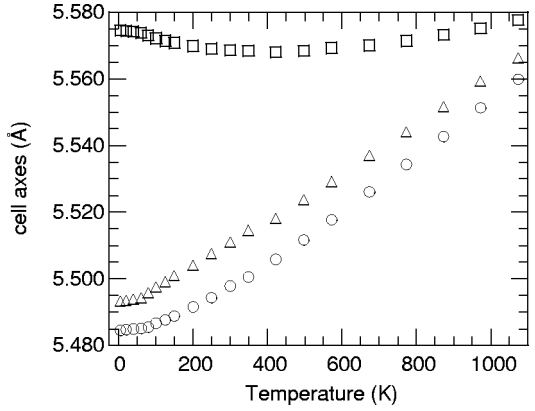

FIG. 2. The temperature dependence of the unit cell axes of (LaCa)$CoRuO_6$. The *b* axis (squares) shows a transition from negative to positive thermal expansion at $T \approx 425$ K, which is accompanied by a slight discontinuity in the *c* axis (triangles). The *a* axis (circles) increases gradually above 100 K.

publication.[6] A second 8 g (LaCa)$CoRuO_6$ sample was prepared following the same procedure. Neutron powder diffraction (NPD) studies were performed on the high-resolution D2B instrument at the Institute Laue Langevin in Grenoble, France. Data were collected in the $8 \leqslant 2\theta \leqslant 160°$ range in 0.05° increments between 4 and 300 K ($\lambda = 1.5946$ Å) and 348–1073 K ($\lambda = 1.5943$ Å). The low-temperature results (4–300 K) have been reported previously.[6] The 348–1073 K data were collected on the second (LaCa)$CoRuO_6$ sample. The GSAS suite of programs[10] was used for Rietveld fitting of the NPD data. A pseudo-Voigt function convoluted with an axial divergence contribution was used to describe the peak shape.

Room temperature XANES measurements were performed at the National Synchrotron Radiation Research Center (NSRRC), Hsinchu Taiwan. Ru L_{III}-edge spectra were recorded in fluorescence mode on beamline BL15B using a modified Lytle detector.[11,12] Both the L_{II} and L_{III} edges of Mo and Pd metallic foils were used to calibrate the photon energies and the AUTOBK code was used for background subtraction. The fitting procedures have been described elsewhere.[10,11]

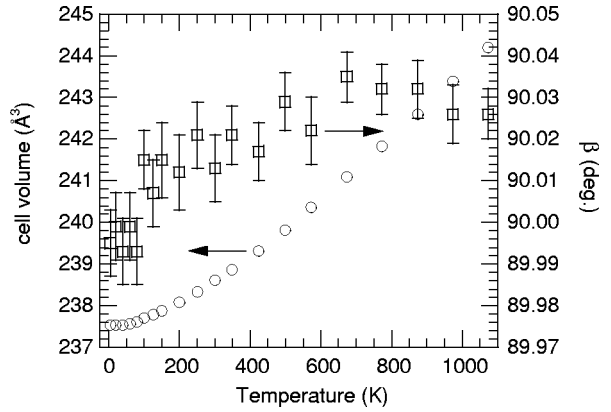

FIG. 3. The temperature dependence of the unit cell volume (circles) and monoclinic angle (squares) of (LaCa)$CoRuO_6$.

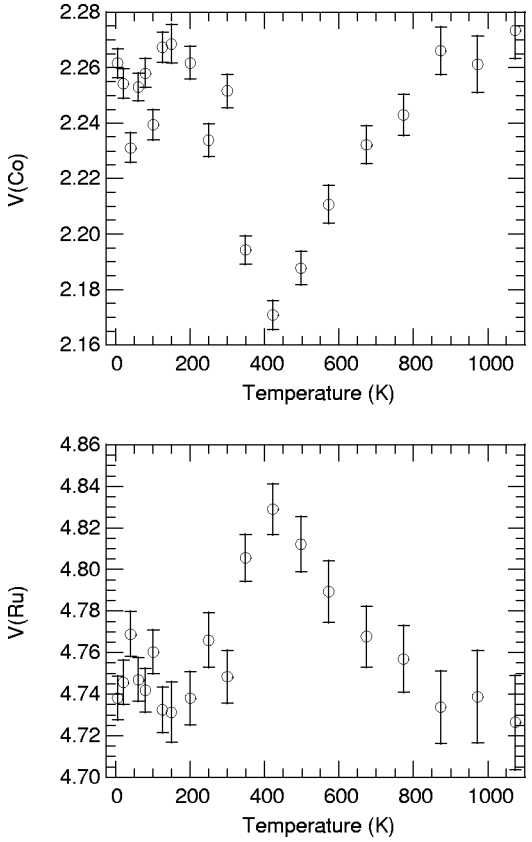

FIG. 4. The thermal evolution of the normalized bond valences for (a) Co and (b) Ru.

III. NEUTRON DIFFRACTION STUDY

The high-temperature study (348–1073 K) was done on the second sample of (LaCa)$CoRuO_6$. Rietveld analyses showed a 4% inversion of Co and Ru (antisite disorder) in this sample, whereas the previously reported first sample (studied at 4–300 K) was fully cation ordered (<1% inversion). However, no discontinuities are observed between 300 and 348 K in any of the structural parameters (Figs. 2–8) when the low- and high-temperature results are combined, so the combination gives a reliable structural evolution of (LaCa)$CoRuO_6$ from 4 to 1073 K. (LaCa)$CoRuO_6$ retains the monoclinic $P2_1/n$ superstructure up to 1073 K and no symmetry-changing phase transitions were observed. The Rietveld fit to the NPD pattern at 1073 K is given in Fig. 1.

The temperature evolution of the lattice constants is given in Figs. 2 and 3. The discontinuities at the Neel transition ($T_N = 96$ K) have been noted in a previous paper,[6] and will be discussed further below. At $T \approx 425$ K, the *b* axis shows a crossover from negative to positive thermal expansion. This is accompanied by a slight discontinuity in the *c* axis. The *a* axis and unit cell volume increase smoothly above 100 K. The monoclinic angle is close to 90° throughout the measured temperature range.

To investigate a possible temperature-dependent Co/Ru valence transfer, bond valence sum (BVS) calculations were performed. BVS's are calculated from the metal-oxygen bond distances (r_i) using the relation

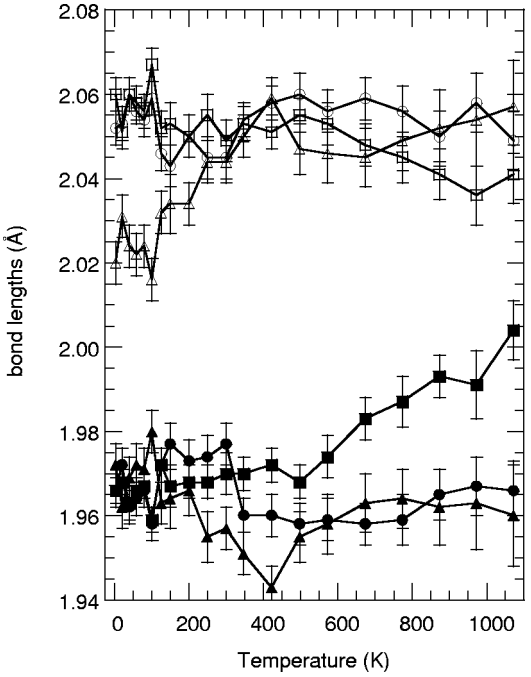

FIG. 5. The temperature evolution of the Co-O and Ru-O bond lengths. M-O1: circles, M-O2: squares, M-O3: triangles, M=Co; open symbols, M=Ru; closed symbols.

$$\mathrm{BVS} = \sum_i \exp(r_o - r_i)/B$$

where B and r_0 are tabulated fitting constants, defined at room temperature.[13] At 300 K, the BVS's confirm the presence of Co^{2+} and Ru^{5+} [BVS's for Co^{2+}=2.35(3) and Ru^{5+} =4.87(7), see Ref. 6]. To eliminate thermal expansion effects over the full temperature range, normalized BVS's are used. These are defined as

$$V(M) = 7\frac{\mathrm{BVS}(M)}{\mathrm{BVS(Co)} + \mathrm{BVS(Ru)}}$$

where M=Co and Ru, BVS(Co) is the BVS for Co^{2+}, and BVS(Ru) is the BVS for Ru^{5+}. The temperature evolutions of the $V(M)$'s are given in Fig. 4. The low- (<200 K) and high-

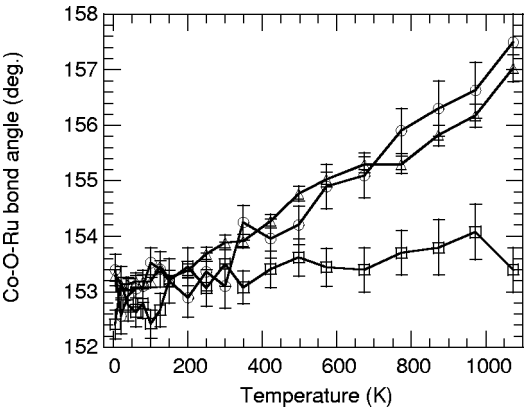

FIG. 6. The temperature evolution of the Co-On-Ru bond angles. O1: circles, O2: squares, O3: triangles.

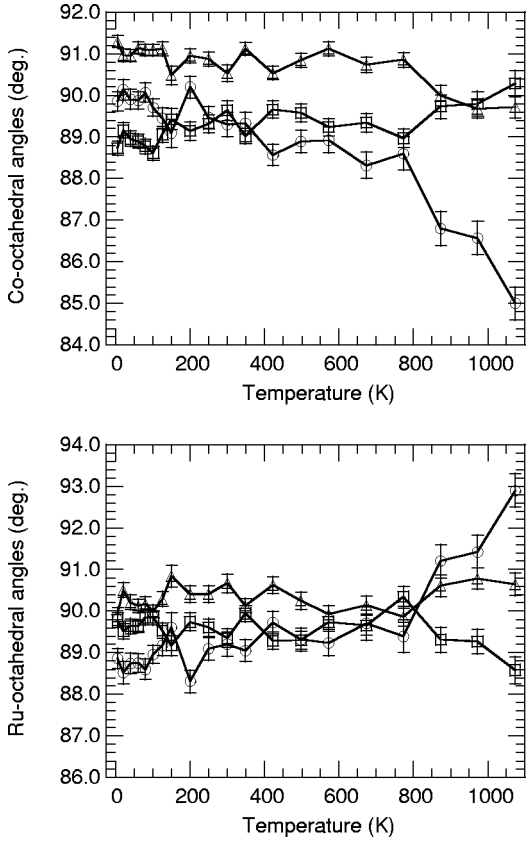

FIG. 7. The temperature evolution of (a) the M=Co and (b) the M=Ru octahedral angles. O1-M-O2: circles, O1-M-O3: squares, O2-M-O3: triangles.

(>800 K) temperature valences converge to asymptotic values of ~2.26 for V(Co) and ~4.74 for V(Ru). In the intermediate temperature range, V(Co) and V(Ru) show a sharp minimum and maximum at $T \approx 425$ K, respectively, coinciding with the broad minimum in b. These extrema are too localized in temperature to represent a true charge transfer, but instead evidence a subtle structural change that results in small deformation of the octahedra.

The thermal variation of the M-O bond distances, bond angles, and octahedral distortion angles are shown in Figs. 5–7. Of the bond distances only the M-O3 bonds show extreme values at $T \approx 425$ K. At 4 K, the CoO_6 octahedra have four long and two short Co-O bonds, while the RuO_6 octahedra are undistorted. The Co-O-Ru bond angles increase smoothly with temperature and the O-M-O angles are almost 90° below 600 K, so the 425 K anomaly is associated specifically with local changes in the M-O3 bond lengths. This is confirmed by the refined oxygen temperature factors, as only O3 shows an anomaly at 425 K (Fig. 8).

As discussed previously (Ref. 6), a common cause for a distortion of octahedral coordination is an orbital ordering resulting from a Jahn-Teller instability. The octahedral Co^{2+} high-spin $3d^7$:$t_{2g}^5 e_g^2$ electronic configuration can be usefully described as $3d^3$:$e_g^2 t_{2g}^1(h)$ hole configuration. This configuration has a triply degenerate ^4T ground state and is susceptible to a Jahn-Teller (orbital ordering) distortion that results in a tetragonal elongation of the CoO_6 octahedra, e.g., for elon-

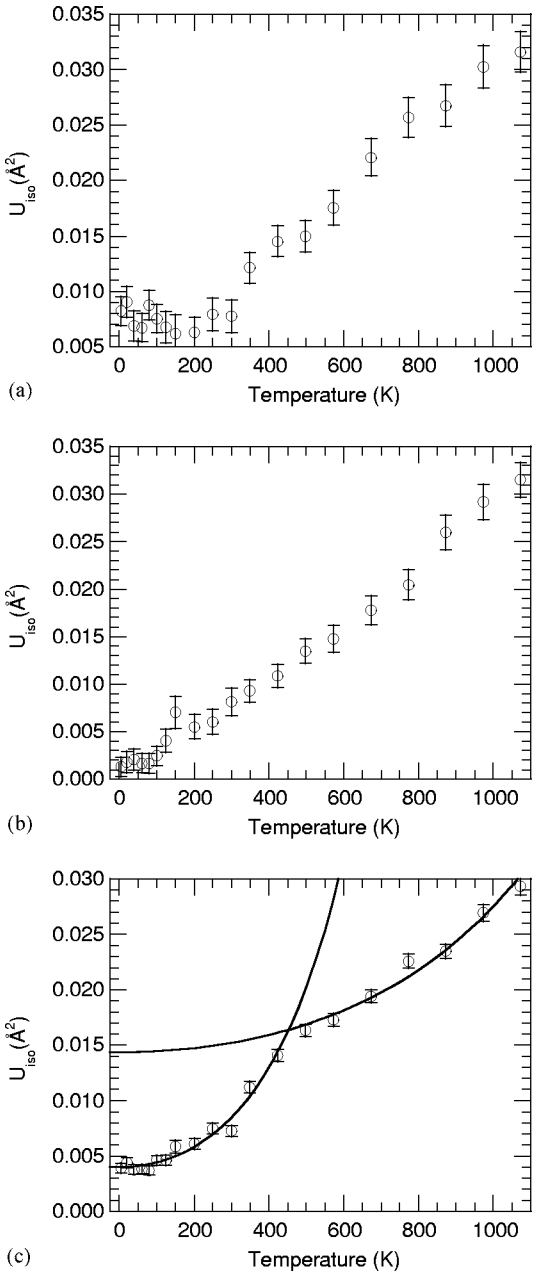

FIG. 8. The thermal variation of the mean squared oxygen displacements for (a) O1, (b) O2, and (c) O3. The solid lines in (c) are fits using $U(T)=U_0\cosh(\alpha T)$ for $T<500$ K and $T>500$ K. U_0 is the mean squared displacement for $T\rightarrow 0$ K and α a fitting constant.

gation along the local z axis, the degeneracy of the $t^1_{2g}(h)$ subshell is removed to give the non degenerate configuration $d^1_{xy}(h)$.

The observed low-temperature distortion is a tetragonal compression, which corresponds to a doubly degenerate $(d_{xz}d_{yz})^1(h)$ configuration that is not a Jahn-Teller mode. This distortion was previously proposed to be magnetostrictive due to the orbital moment of high-spin Co^{2+} (Ref. 6). However, the high-temperature neutron data support another explanation based on the presence of a partial orbital ordering (OO) that occurs when cooling below $T\approx 425$ K. At high temperatures, the three possible orbital hole states $[d^1_{yz}(h)$, $d^1_{xz}(h)$ and $d^1_{xy}(h)]$ are equally populated and the elongated axes of the CoO_6 octahedra are distributed statistically among the [110], [$\bar{1}$10], and [001] directions. This results in six equally long average Co-O bonds (Fig. 5). At 425 K, a partial OO occurs such that the $d^1_{xy}(h)$ state becomes depopulated, resulting in elongation of bonds in only the [110] and [$\bar{1}$10] directions. This is observed as tetragonally compressed CoO_6 octahedra at low temperatures (Fig. 5).

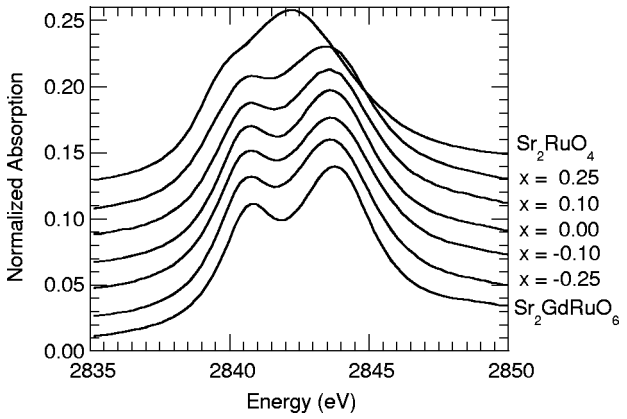

FIG. 9. The Ru L-edge x-ray absorption spectra of $(La_{1+x}Ca_{1-x})CoRuO_6$ and reference materials. Spectra are offset by 0.02 units of absorption.

This partial OO is also evidenced by the mean squared oxygen displacement for O3 [Fig. 8(c)]. The difference in root mean squared displacement between the extrapolated high (0.014 Å^2) and low (0.004 Å^2) temperature U_{iso} limits is 0.05 Å, which is comparable to the observed decrease of the Co-O3 bond length (0.04 Å).

Subtle, partial OO of this type is rarely seen due to the small magnitude of the structural distortions for T-state ions and the lack of a symmetry-breaking transition, but may be common. Larger structural distortions are found in systems where OO of the e_g states occurs, such as in the manganites. The onset of long-range magnetic ordering at 96 K enhances the structural distortions associated with the OO through a magnetostrictive effect observed previously. This may signify the complete depopulation of the $d^1_{xy}(h)$ state below T_N.

IV. Ru XANES MEASUREMENTS

The Ru L-edge XANES spectra of the $(La_{1+x}Ca_{1-x})CoRuO_6$ $(-0.25\leqslant x\leqslant 0.25)$ double perovskites are given in Fig. 9. The perovskite-related materials Sr_2RuO_4 and Sr_2GdRuO_6 were used as reference materials for Ru^{4+} and Ru^{5+}, respectively. The shape and position of the $(La_{1+x}Ca_{1-x})CoRuO_6$ Ru L-edges closely resemble that of Sr_2GdRuO_6, indicating dominant Ru^{5+} character. The positions of the absorption edges were used to estimate the Ru valence state, giving an estimate of +4.90 for Ru in the undoped ($x=0$) composition. Comparison with values from the other samples (Fig. 10) enables the doping mechanism to be determined, and shows whether the latter value represents a small Ru/Co charge transfer.

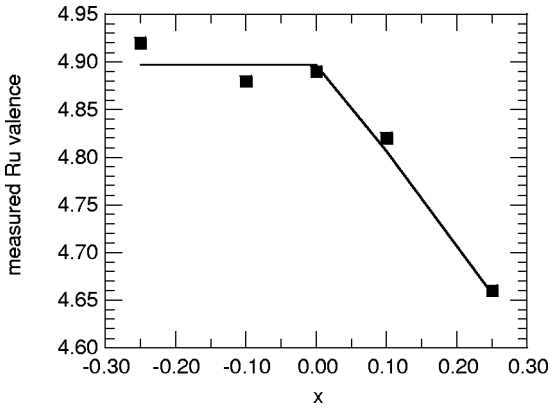

FIG. 10. The measured Ru valences for $(La_{1+x}Ca_{1-x})CoRuO_6$ as determined from XANES. The lines show the variation expected for the chemical model discussed in the text, with an offset of 0.1 between the formal and measured Ru valences.

In a simple chemical model for doping effects in $(La_{1+x}Ca_{1-x})CoRuO_6$,[6] excess La substitution ($x>0$) results in the partial reduction $Ru^{5+}\rightarrow Ru^{4+}$ through electron doping of $Ru:t_{2g}$ bands while excess Ca ($x<0$) leads to the partial oxidation of $Co^{2+}\rightarrow Co^{3+}$ from hole doping of $Co:e_g$ bands while the Ru valence remains as +5. The x dependence of the Ru valence derived from the XANES measurements is shown in Fig. 10. The results are in excellent agreement with the predictions of the chemical model. For $x\leqslant 0$, near constant valences are found, while for $x>0$, the Ru valence decreases linearly with x. Hence the limiting value of +4.90 for $x\leqslant 0$ corresponds to the formal Ru^{5+} state, showing that there is no Ru/Co charge transfer at $x=0$. The asymmetry (with respect to x) in the magnetic and transport properties of $(La_{1+x}Ca_{1-x})CoRuO_6$ (Ref. 6) results from the asymmetric doping mechanism demonstrated by this XANES study.

V. CONCLUSIONS

The variable temperature NPD study of $(LaCa)CoRuO_6$ reveals a crossover from negative to positive thermal expansion of the b axis at $T\approx 425$ K accompanied by a discontinuity in the c axis. Sharp extrema in the normalized BVS's at $T\approx 425$ K are associated with a subtle orbital ordering transition rather than Co/Ru charge transfer. The transition is driven by the Jahn-Teller instability of the high-spin Co^{2+} cations. Above 425 K, the $d^1_{yz}(h)$, $d^1_{xz}(h)$, and $d^1_{xy}(h)$ orbital hole states are equally populated. Below 425 K, a partial orbital ordering occurs, such that the $d^1_{xy}(h)$ state becomes depopulated and the Co—O3 bond is shortened resulting in tetragonally compressed CoO_6 octahedra. The Ru valence states of the $(La_{1+x}Ca_{1-x})CoRuO_6$ ($-0.25\leqslant x\leqslant 0.25$) materials derived from XANES spectroscopy confirm that Ru^{5+} is present at $x=0$ and support the asymmetric chemical doping model. For $x\leqslant 0$ compositions a constant Ru^{5+} state is maintained, but Ru^{5+} is reduced for $x>0$ through electron doping of the $Ru:t_{2g}$ bands.

ACKNOWLEDGMENTS

J.P.A. and J.W.G.B. thank the EPSRC for neutron beamtime at the ILL and Dr. E. Suard for help with data collection. J.W.G.B. acknowledges support from the EPSRC. T.S.C. and R.S.L. acknowledge the financial support from the national science council of Taiwan and the Ministry of Economic Affairs of Taiwan under Grant Nos. 93-2113-M-002-006 and 93-EC-17-A-08-S1-0006, respectively.

[1] M. T. Anderson, K. B. Greenwood, G. A. Taylor, and K. R. Poeppelmeier, Prog. Solid State Chem. **22**, 197 (1993).
[2] K. L. Kobayashi, T. Kimura, H. Sawada, K. Terakura, and Y. Tokura, Nature (London) **395**, 677 (1998).
[3] J. Gopalakrishnan, A. Chattopadhyay, S. B. Ogale, T. Venkatesan, R. L. Greene, A. J. Millis, K. Ramesha, B. Hannoyer, and G. Marest, Phys. Rev. B **62**, 9538 (2000).
[4] D. D. Sarma, Curr. Opin. Solid State Mater. Sci. **5**, 261 (2001).
[5] H. van Leuken and R. A. de Groot, Phys. Rev. Lett. **74**, 1171 (1995).
[6] Jan-Willem G. Bos, and J. P. Attfield, Phys. Rev. B **69**, 094434 (2004).
[7] J. W. G. Bos and J. P. Attfield, Chem. Mater. **16**, 1822 (2004).
[8] S. H. Kim and P. D. Battle, J. Solid State Chem. **114**, 174 (1995).
[9] J. W. G. Bos and J. P. Attfield, J. Mater. Chem. **15**, 715 (2005).
[10] A. C. Larson and R. B. von Dreele, General Structural Analysis System (GSAS), report LAUR 86-748, Los Alamos National Laboratory (1994).
[11] R. S. Liu, L.-Y. Jang, H. H. Hung, and J. L. Tallon, Phys. Rev. B **63**, 212507 (2001).
[12] G. V. M. Williams, L.-Y. Jang, and R. S. Liu, Phys. Rev. B **65**, 064508 (2002).
[13] I. D. Brown, Acta Crystallogr., Sect. B: Struct. Sci. **B48**, 553 (1992).